

pubs.acs.org/cm Article

Two Metal Phosphate Nonlinear Optical Materials Simultaneously Exhibiting Ultraviolet Transparence and a Large Birefringence

Jiarong Lv, Yanyan Qian, Qun Jing,* Xinmei Wang, Ming-Hsien Lee, and Zhaohui Chen*



Cite This: Chem. Mater. 2022, 34, 5919-5927



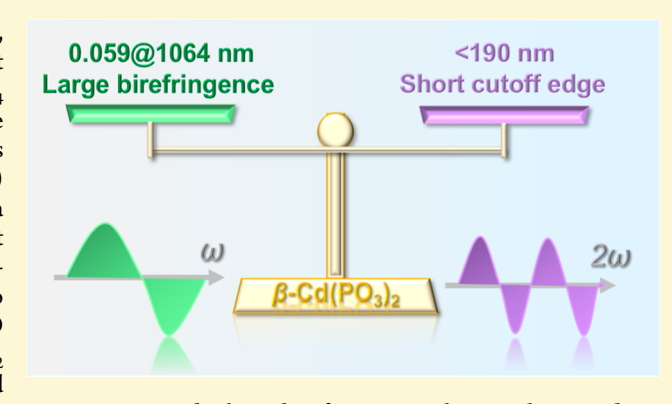
ACCESS

Metrics & More

Article Recommendations

Supporting Information

ABSTRACT: For phosphate nonlinear optical (NLO) materials, how to improve their small birefringence is confronted with a great contradiction of their weak optical anisotropy of tetrahedral PO₄ groups. Herein, by introducing La³⁺ with a closed-shell structure and Cd²⁺ with a d¹⁰ electronic configuration, two NLO materials with a large birefringence, namely, La(PO₃)₃ (0.040@1064 nm) and β-Cd(PO₃)₂ (0.059@1064 nm), have been synthesized by a high-temperature solution method. In particular, for β-Cd(PO₃)₂, it possesses the largest birefringence among the known deepultraviolet (DUV) phosphates to date, which is attributed to cooperative effects of strong covalence of Cd–O groups and P–O pseudolayers similar to those of a plane. Meanwhile, β-Cd(PO₃)₂ exhibits the shortest cutoff edge (<190 nm) among the reported



Cd-based inorganic compounds and realizes a balance between DUV transparence and a large birefringence. This insight provides a new opportunity to design high-performance NLO materials using metal phosphates.

1. INTRODUCTION

Nonlinear optical (NLO) materials are in great demand for generating deep ultraviolet (DUV, < 200 nm) coherent light and therefore attract plenty of attention for potential application in laser micromachining, material-processing, photolithography, optical measurements, and manipulating entangled photons. A quintessential DUV NLO crystal should possess several characteristics, such as (i) a non-centrosymmetric (NCS) structure, (ii) a short UV cutoff edge and a wide transparent region, and (iii) a large NLO coefficient [more than 1× KH₂PO₄ (KDP)] and appropriate birefringence. Appropriate birefringence is crucial for the application of an NLO crystal due to its impact on the phase-matching angle and wavelength range.

Traditionally, in order to obtain sufficient birefringence for NLO crystals, planar building units with π_6^4 characteristic orbits are often employed, $^{12-14}$ such as $[BO_3]^{3-}$, $[CO_3]^{2-}$, and $[NO_3]^-$ groups, which maintain outstanding anisotropies to accomplish adequate birefringence via π -conjugated molecular orbital interactions. $^{15-18}$ Recently, continuous studies have resulted in some preeminent DUV NLO materials with large birefringence, such as AB_4O_6F (A = NH_4 , Na, Rb, and Cs), $^{19-22}$ $CsZn_2BO_3X_2$ (X = F and Cl), 23 $NaZnCO_3(OH)$, and Cs0 Cs1.

For comparison, non- π -conjugated phosphates, sulfates, and silicates are also deemed promising candidates, attributed to their remarkable impervious absorption and varieties of crystal structures. ^{26–31} In particular, regarding phosphates, a tetrahedral chromophore PO₄ has a broad energy gap between the

lowest unoccupied molecular orbital and the highest occupied molecular orbital and shows dominance in search of DUV NLO materials. For instance, BPO₄ possesses an eminent short cutoff edge (about 130 nm), but its birefringence is exceedingly small (0.0052@1014 nm), which generates the shortest phase matching (PM) wavelength beyond 532 nm and hampers the application in the DUV region. Hurthermore, the dispersive curves of refractive indexes become indeed steeper with the decrease of wavelength, and, consequently, a larger birefringence with optimized refractive index dispersion is demanded to achieve phase-matching. Therefore, how to improve the birefringence of DUV phosphates is an urgent dilemma.

Commonly, d^0/d^{10} metals and stereo-chemically active lone pair cations (such as Mo^{6+} , W^{6+} , Hg^{2+} , Pb^{2+} , Te^{4+} , Bi^{3+} , Sb^{3+} , Ti^{4+} , etc.) are introduced into phosphates to ameliorate birefringence, for example, $KCsAP_2O_9$ (A = Mo and W), 36,37 LiHgPO₄, 38 A₃BBi(P₂O₇)₂ (A = Rb and Cs; B = Pb and Ba), 39,40 Pb₃Mg₃TeP₂O₁₄, 41 and $K_2Sb(P_2O_7)F$. 42 Nevertheless, this may be accompanied by a red shift of the UV cutoff edge. 43 An instance is $KTiOPO_4$ (KTP), which expresses

Received: March 18, 2022 Revised: June 11, 2022 Published: June 24, 2022





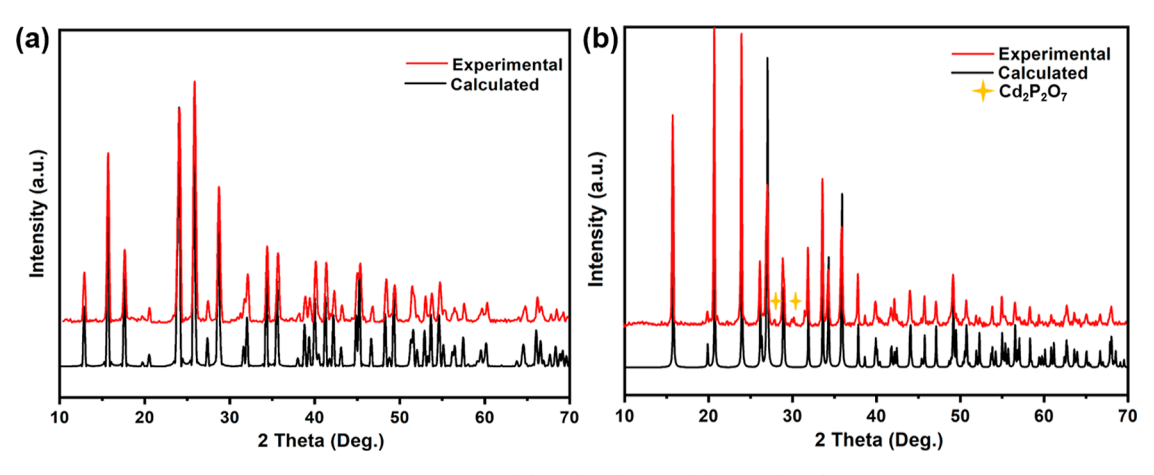


Figure 1. Calculated and experimental powder XRD patterns of (a) La(PO₃)₃ and (b) β -Cd(PO₃)₂.

gigantic birefringence (0.09@1064 nm) due to aligned arrangement of the second-order Jahn–Teller-distorted TiO₆ octahedra, but the UV cut-off edge of KTP is 350 nm. ^{44,45} In order to harmonize the cutoff edge and birefringence, we import the following cations: (i) Rare-earth cations with a closed shell structure, ensuring the short UV cutoff edge and (ii) d¹⁰ cations with considerable polarizability, restraining the d–d electron transition effectively. Under the guidance of the above idea, we successfully synthesized two NLO materials, La(PO₃)₃ and β -Cd(PO₃)₂. Of them, β -Cd(PO₃)₂ realized the harmony of large birefringence and DUV transparence. As far as we know, it possesses the largest birefringence (0.059 at 1064 nm) in DUV phosphates and the shortest UV cutoff edge (<190 nm) in all reported Cd-based inorganic compounds.

2. METHODS

- **2.1. Reagents.** La_2O_3 (99.9%), Rb_2CO_3 (99.8%), CdO (99%), $NH_4H_2PO_4$ (99%), and PbO (99.9%) were purchased from Aladdin Chemical Co., Ltd.
- **2.2. Synthesis.** La(PO₃)₃ and β -Cd(PO₃)₂ were synthesized by high-temperature solid-state reaction. Some powder samples of La(PO₃)₃ were prepared from stoichiometric molar ratio raw materials of La₂O₃ (6.519 g) and NH₄H₂PO₄ (13.803 g). The mixture was mixed in and triturated fully with an agate mortar and preheated up to 300 $^{\circ}\text{C}$ for 24 h to discharge H_2O and NH_3 in a muffle furnace. Then, it was heated to 750 °C successively and held for 72 h at the selected optimum temperature with some intermediate grindings and mixings. The polycrystalline sample of β -Cd(PO₃)₂ was also synthesized in a similar way. Differently, CdO (8.989 g) and NH₄H₂PO₄ (16.104 g) were mixed and held for 60 h at 860 °C. They were then quickly removed from the muffle furnace and quenched in an air-cooled environment [do not let it slowly cool in the muffle furnace, or it will turn into $\alpha\text{-Cd}(PO_3)_2$]. We can increase the degree of supercooling by quenching, which effectively inhibited its phase transformation. Finally, the polycrystalline sample of β -Cd(PO₃)₂ was obtained successfully.
- **2.3. Single-Crystal Growth.** Crystals of La(PO₃)₃ were synthesized via a high-temperature solution method. The reagents La₂O₃, NH₄H₂PO₄, Rb₂CO₃, and PbO were mixed in a 1:4:1:1 M ratio, and Rb₂CO₃ and PbO were used as flux agents. The mixture was ground completely and packed into a platinum crucible. It was heated to 920 °C from room temperature and held at the temperature for 12 h to obtain a transparent melt and then was cooled slowly to 620 °C with 2 °C/h. After that, the melt was cooled rapidly to room temperature with 10 °C/h. The crystals of β-Cd(PO₃)₂ were grown by a similar temperature procedure. Differently, the reagents of β-Cd(PO₃)₂ were CdO and NH₄H₂PO₄ in stoichiometric molar ratios. They were held at 900 °C for 12 h, and then, they were cooled slowly to 600 °C with 2 °C/h. Then, the furnace was turned off and allowed

Table 1. Crystal Data and Structure Refinements for La(PO₃)₃ and β-Cd(PO₃)₂

empirical formula	$La(PO_3)_3$	β -Cd(PO ₃) ₂					
formula weight	375.82	270.34					
temperature/K	296.15	296.15					
wavelength/Å	0.71073	0.71073					
crystal system	orthorhombic	orthorhombic					
space group	C222 ₁ (no. 20)	P2 ₁ 2 ₁ 2 ₁ (no. 19)					
a (Å)	8.6382(10)	7.3128(5)					
b (Å)	11.2850(12)	7.3969(6)					
c (Å)	7.3812(8)	8.5631(7)					
volume ($Å^3$), Z	719.53(14), 4	463.20(6), 4					
calculated density (Mg/m^3)	3.469	3.877					
$ \begin{array}{c} \text{absorption} \\ \text{coefficient } \left(\text{mm}^{-1}\right) \end{array} $	6.628	5.350					
F(000)	696	504					
crystal size (mm ³)	$0.14 \times 0.12 \times 0.09$	$0.21\times0.16\times0.10$					
theta range for data collection (deg)	2.970 to 27.502	3.640 to 30.553					
limiting indices	$-11 \le h \le 11, -14 \le k$ $\le 14, -9 \le l \le 8$	$-10 \le h \le 10, -10 \le k \le 10, -11 \le l \le 12$					
reflections collected/ unique	$7963/839 [R_{(int)} = 0.0673]$	$7272/1417 [R_{(int)} = 0.0368]$					
completeness (%)	100.0	99.8					
data/restraints/ parameters	839/0/62	1417/0/103					
goodness-of-fit on F_o^2	1.077	1.055					
final R indices $[F_o^2 > 2\sigma(F_o^2)]^a$	$R_1 = 0.0177, \ wR_2 = 0.0388$	$R_1 = 0.0233, wR_2 = 0.0441$					
R indices (all data) ^a	$R_1 = 0.0185, \ wR_2 = 0.0392$	$R_1 = 0.0256$, $wR_2 = 0.0446$					
absolute structure parameter	0.49(3)	0.02(2)					
refinement method	full-matrix least-squares on F^2						
extinction coefficient	n/a	0.0015(5)					
largest diff. peak and hole $(e \cdot \mathring{A}^{-3})$	0.502 and -0.536	1.373 and -0.911					
${}^{a}R_{1} = \Sigma F_{o} - F_{c} /\Sigma F_{o} $ and $wR_{2} = \left[\Sigma w (F_{o}^{2} - F_{c}^{2})^{2}/\Sigma w F_{o}^{4}\right]^{1/2}$ for $F_{o}^{2} > 2\sigma(F_{o}^{2})$.							

to cool naturally to room temperature. Finally, some block, clear

crystals (Figure S1) were gained for structure determination. **2.4. Powder X-Ray Diffraction.** Powder X-ray diffraction (PXRD) analysis of La(PO₃)₃ and β -Cd(PO₃)₂ was performed employing a Bruker D2 Advance X-ray Diffractometer with Cu-K α radiation (λ = 1.5418 Å). The scanning step size was 0.02°/s at 298

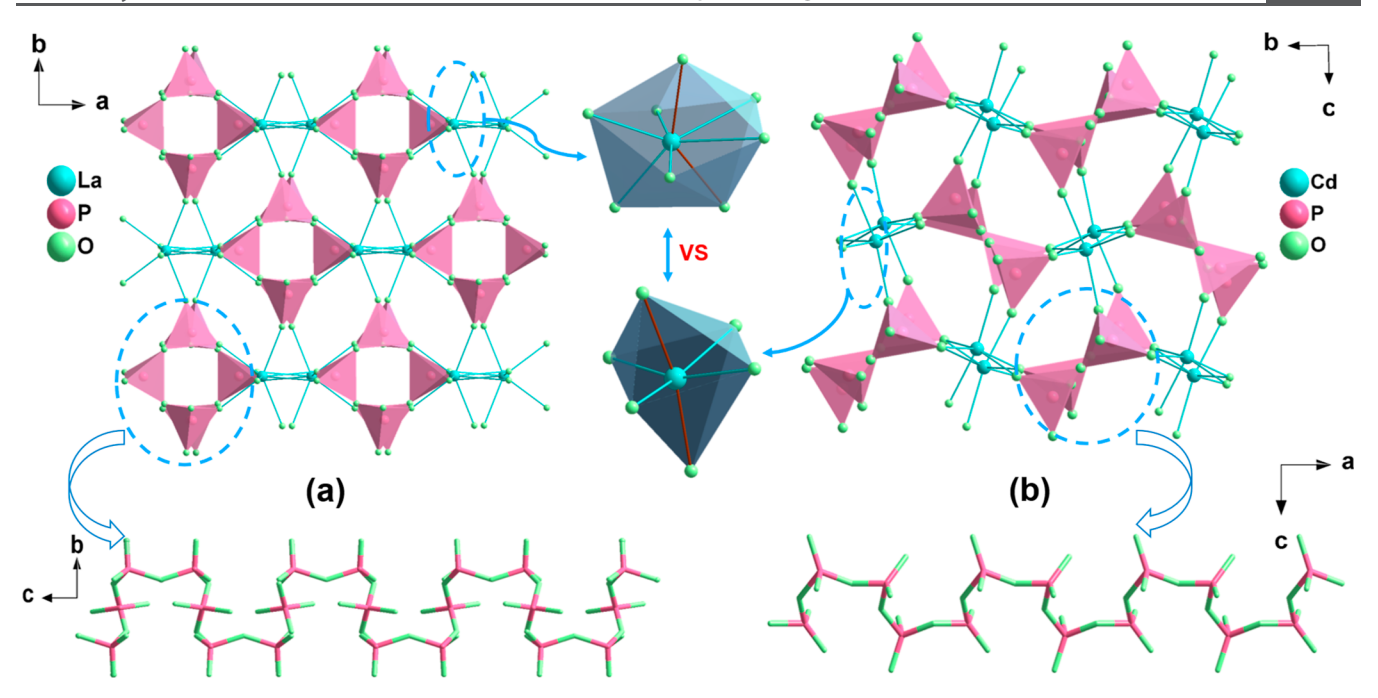


Figure 2. Crystal structures of (a) $La(PO_3)_3$ viewed along the [001] direction and (b) β -Cd(PO₃)₂ viewed along the [100] direction.

K. As Figure 1 shown, experimental powder XRD patterns of the two compounds agreed with the calculated ones.

2.5. Single-Crystal X-Ray Diffraction. The clear crystals closing to $0.16 \times 0.09 \times 0.05 \text{ mm}^3$ for $\text{La}(\text{PO}_3)_3$ and $0.21 \times 0.16 \times 0.10 \text{ mm}^3$ for β -Cd(PO₃)₂ were selected for single-crystal XRD. All data were collected on a Bruker D8 Advance X-ray diffractometer with Mo K α radiation (λ = 0.71073 Å), and absorption correction use the SAINT program. All atom positions were decided by direct approach in the SHELXL-2016 system. The structures were inspected for missing symmetry elements with PLATON. The detailed crystal structure data are compiled in Table 1. Atomic coordinate-equivalent isotropic displacement parameters, selected bond lengths, and anisotropic displacement parameters are exhibited in Tables S1–S6.

2.6. Thermal Behavior Analysis. Thermal gravimetric (TG) and differential thermal analysis (DTA) were determined on the HITACHI STA 7300 thermal analyzer at a rate of 10 °C/min under flowing nitrogen gas from 30 to 900 °C

2.7. Spectroscopy Analysis. Infrared (IR) spectra of La(PO₃)₃ and β -Cd(PO₃)₂ were obtained using the BRUKER VERTEX 70 spectrometer with a wavelength range 400 to 4000 cm⁻¹. The UV–vis–NIR diffuse reflectance data of La(PO₃)₃ and β -Cd(PO₃)₂ were collected using a Shimadzu DUV-3700 spectrophotometer with a wavelength range from 180 to 2600 nm at room temperature.

2.8. Elemental Analysis. Microprobe elemental analytical data and distribution diagrams were acquired on a LEO-1430VP scanning electron microscope. For β -Cd(PO₃)₂, the experimental weight ratios of O, P, and Cd were 34.31, 23.62, and 42.07%; for La(PO₃)₃, the analyzed weight ratios of O, P, and La were 38.62, 24.61,and 36.77%. They were all coincident with the theoretical amounts (Figure S2).

2.9. Second-Harmonic Generation Measurements. Since $La(PO_3)_3$ and β -Cd $(PO_3)_2$ crystallized in NCS space groups, the powder second-harmonic generation (SHG) responses were enforced on a Q-switched Nd: YAG laser at a wavelength of 1064 nm by the Kurtz–Perry approach. Because the SHG intensity was dependent on the speck size, polycrystalline samples were milled and selected based on the following particle sizes: 20-38, 38-55, 55-88, 88-105, 105-150, 150-200, and $200-250~\mu m$. The samples were squeezed between two glass slides and attached in 1 mm thick aluminum holders with an 8 mm diameter gap. After that, the samples were deposited into a light-tight box and illuminated with pulsed laser. The intensity of frequency-doubled output was gathered by a photo-

multiplier tube. The known SHG KDP and SiO₂ samples with the same speck ranges were used as references.

2.10. Details of Calculation. The electronic structures and optical properties of $La(PO_3)_3$ and β -Cd $(PO_3)_2$ were calculated using the density functional theory (DFT) implemented in the plane wave pseudopotential CASTEP package. The exchange—correlation effect was adopted by the generalized gradient approximation with the Perdew—Burke—Ernzerhof 52,53 functional. The valence electrons were set as $La:5d^16s^2$, $Cd:4d^{10}5s^2$, $P:3s^23p^3$, and $O:2s^22p^4$ by the norm-conserving pseudopotentials. 54,55 To achieve energy convergence, the cutoff energy of $La(PO_3)_3$ and β -Cd $(PO_3)_2$ was set at 830 eV. Monkhorst—Pack k-point mesh with densities of $4 \times 4 \times 3$ and $3 \times 3 \times 3$ in the Brillouin zone was used for $La(PO_3)_3$ and β -Cd $(PO_3)_2$, respectively. The refractive indices and birefringence were further calculated by the OptaDOS code. 56,57 The SHG tensors of $La(PO_3)_3$ and β -Cd $(PO_3)_2$ were further investigated using the method described in ref 58 With regards to other calculation arguments and convergent conditions, we used defaults of the CASTEP code.

3. RESULTS AND DISCUSSION

3.1. Crystal Structure. The crystal structures of La(PO₃)₃ and β -Cd(PO₃)₂ are assigned to space groups C222₁ (no. 20) and P2₁2₁2₁ (no. 19), respectively. The asymmetric units consist of one La, two P, and five O atoms for La(PO₃)₃ and one Cd, two P, and six O atoms for β -Cd(PO₃)₂ (Tables S1, S2). The two compounds are known, 59,60 so only their distinctive structural features are discussed here. As depicted in Figure 2, they contain analogous structures with the onedimensional $[PO_3]_{\infty}$ chain, which is further linked by distorted [LaO₈] Iso isal or [CdO₆] octahedra into a three-dimensional network. Interestingly, each La/Cd-O group combines four [PO₃]_∞ chains around it (up, down, left, and right). Among them, six La-O bonds (turquoise bonds in Figure 3a) connect to left and right chains along the a axis, while two La-O bonds (brown bond in Figure 3a) connect to up and down chains along the b axis. A similar coordination circumstance also appears in β -Cd(PO₃)₂ (Figure 3b). We regard the connection of $[LaO_8]$ lso isal $([CdO_6]$ octahedra) with $[PO_3]_{\infty}$ chains along the a axis (b axis) as a pseudolayer (Figure 3c,d) and continue to analyze the relationship between the crystal

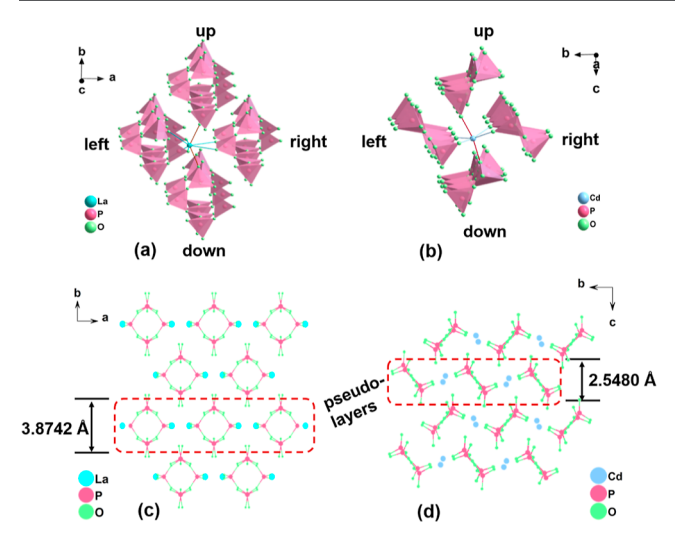


Figure 3. (a) $[PO_3]_{\infty}$ chains connected with $[LaO_8]$ polyhedron and $[CdO_6]$ octahedron. For $La(PO_3)_3$, up and down chains stack along the b axis, and left and right chains stack along the a axis. For β- $Cd(PO_3)_2$, up and down chains stack along the c axis and left and right chains stack along b axis. Pseudolayers of (c) $La(PO_3)_3$ and (d) β- $Cd(PO_3)_2$. Pseudolayers stack along the b axis in $La(PO_3)_3$. Pseudo-layers stack along the c axis in β- $Cd(PO_3)_2$.

structure and birefringence in the following paragraph. The bond valence sums (BVS) of La^{3+} , Cd^{2+} , P^{5+} , and O^{2-} are listed in Tables S1, S2, indicating that the structure models are reasonable and correct.

3.2. Relationship between Birefringence and Crystal Structures. The refractive indices and birefringence of $La(PO_3)_3$ and β -Cd(PO₃)₂ are estimated using first-principles calculations. As shown in Figure 4a,b, they belong to negative biaxial and positive biaxial crystals, respectively. The birefringence $(\Delta n = n_z - n_x)$ is 0.040 for $La(PO_3)_3$ and 0.059 for β -Cd(PO₃)₂ at 1064 nm.

Especially, the birefringence of β -Cd(PO₃)₂ represents the largest value for DUV phosphates to date (Table 2). In order to trace the origin of large birefringence, the real-space atom cutting (RSAC) method is applied.⁶⁷ In the RSAC process, we keep atomic spheres in contacting with each other without overlapping. For La(PO₃)₃ and β -Cd(PO₃)₂, the cutting radii are set as follows: 1.30 Å (La), 1.00 Å (Cd), 0.95 Å (P), and 1.10 Å (O). According to the atomic coordination environment, the threshold of chemical bond was set as 3.5 Å. As displayed in Figure 5 and Table S7, birefringence of the title compounds is essentially contributed by PO₄ units, and La/ Cd-O lso isal also exhibit an appreciable contribution, which is consistent with the reported results; that is, the strong covalent interaction should influence birefringence.⁶⁸ Thereupon, we figure out the Mulliken bond populations of $La(PO_3)_3$ and β -Cd(PO₃)₂ (Table S8). In addition to a large degree overlap for P-O bonds, La/Cd-O bonds also appear to show impressive covalent interaction, which is consistent with the outcome of RSAC operation. According to the Pauling electronegativity scale, ⁶⁹ the electronegativity of Cd (1.7) is greater than that of La (1.1), and the electronegativity difference between Cd and O (1.8) is less than that of La and

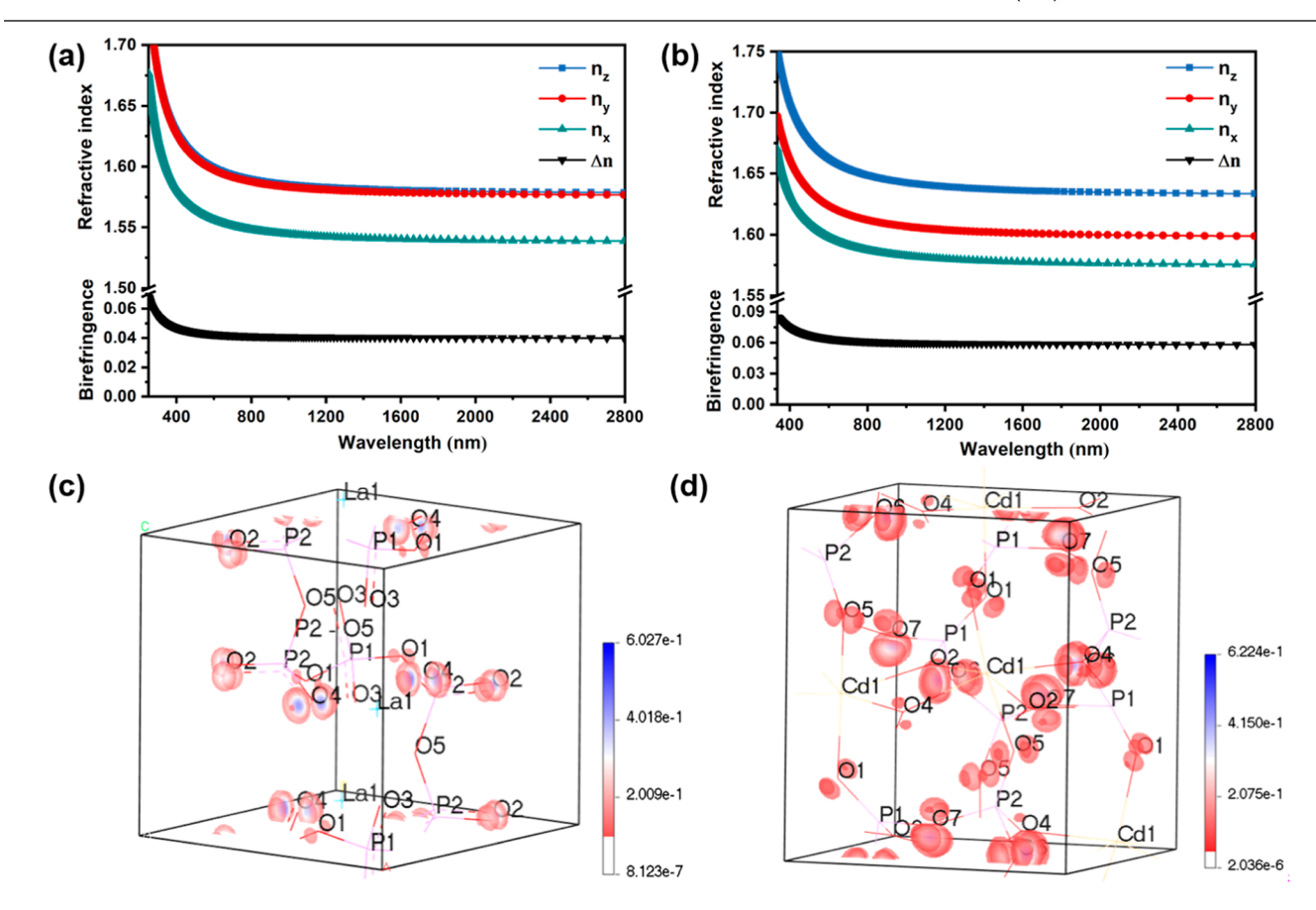


Figure 4. Refractive indices and birefringence of (a) La(PO₃)₃ and (b) β -Cd(PO₃)₂ at 1064 nm. Orbital electron density maps of (c) La(PO₃)₃ and (d) β -Cd(PO₃)₂ nearing the Fermi level.

Table 2. Optical Properties of Some DUV NLO Phosphates^a

compound	space group	cut-off edge (nm)	birefringence	reference
$RbBa_2(PO_3)_5$	Pc	163	N/A	32
$Rb_2Ba_3(P_2O_7)_2$	$P2_{1}2_{1}2_{1}$	<200	N/A	32
$CsLa(PO_3)_4$	$P2_1$	<167	0.0068@ 1064nm	61
KLa(PO ₃) ₄	$P2_1$	<162	0.0084@ 1064nm	62
$\mathrm{K_4Mg_4(P_2O_7)_3}$	Pc	170	0.0108@ 1064nm	63
$K_2SrP_4O_{12}$	$I\overline{4}$	<200	0.016@ 1064nm	64
Ba ₂ NaClP ₂ O ₇	P4bm	<176	0.017@1064 nm	28
$Ba_3P_3O_{10}Br$	$P2_12_12_1$	<200	0.023@ 1064nm	26
$Ba_3P_3O_{10}Cl$	$Pca2_1$	180	0.028@ 1064nm	26
$(NH_4)_2PO_3F$	$Pna2_1$	<177	0.03@589.3 nm ^b	9
$RbNaMgP_2O_7(LTP)$	$Pna2_1$	185	0.031@ 532nm	33
KDP (KH_2PO_4)	I 4 2d	176	0.034@1064 nm	65
$RbNaMgP_2O_7(HTP)$	$Ccm2_1$	185	0.035@ 532nm	33
$NaNH_4PO_3F{\cdot}H_2O$	Pc	<176	0.053@ 589.3nm ^b	66
β -Cd(PO ₃) ₂	P 2 ₁ 2 ₁ 2 ₁	<190	0.059@ 1064 nm	this work

^aN/A = not reported or not available. ^bValues observed experimentally.

O (2.4). Moreover, from the bonding orbital (Figure 4c,d) of La–O and Cd–O, the covalent interaction of Cd–O bonds is stronger than that of La–O. Therefore, the large birefringence of the title compounds comes from the synergistic effect of P–O and La/Cd–O bond covalent interaction.

Although both materials manifest large birefringence, there is still a non-ignorable disparity, which is particularly crucial for phosphates. As mentioned above, the left and right $[PO_3]_{\infty}$ chains along the a axis are connected closely for both compounds, so we assume them as pseudolayers stacking along the [010] direction for $La(PO_3)_3$ (Figure 3c) and [001] direction for β -Cd(PO_3)₂ (Figure 3d). By comparing, it can be found that P-O pseudolayer thickness of β -Cd(PO_3)₂ (2.5480 Å) is much smaller than that of $La(PO_3)_3$ (3.8742 Å), which

results P–O pseudolayers of β -Cd(PO₃)₂ that are more conducive to a plane. In other words, the undulation of P–O pseudolayers is feebler in β -Cd(PO₃)₂, which strengthens structural anisotropy, therefore enlarging birefringence. Besides, dipole moments can roughly reflect the distortion degree of the functional group and is conducive to comprehend the origin of large birefringence. Therefore, the local dipole moments of [LaO₈] and [CdO₆] lso isal are calculated by the Debye equation, $\mu = qd$, where μ is the dipole moment, q is the normalized net charge, and d is the distance between the ions. The result displays that the dipole moment of [CdO₆] octahedra is larger than that of [LaO₈] lso isal (Table S9), which also heightens the birefringence of the β -Cd(PO₃)₂ compound.

3.3. Thermal Behavior Analysis. TG–DTA curves of the title compounds are marked in Figure 6a,d. For TG curves, there is no obvious weight loss up to 1000 °C. On the DTA curve of La(PO₃)₃, no detecting peak appears in either the heating or cooling process, signifying that the material has good thermal stability. For β -Cd(PO₃)₂, the endothermic peak at 821 °C and the exothermic peak at 446 °C may indicate the phase temperature according to previous research. Another endothermic peak at 878 °C corresponds to the melting point, which is basically close to that observed in crystal growth experiment.

3.4. Optical Properties. IR spectra of La(PO₃)₃ and β -Cd(PO₃)₂ are plotted in Figure 6b,e. It is apparent that their IR spectra possess a certain degree of resemblance. Peaks nearby 1274 cm⁻¹ for La(PO₃)₃ and 1282 cm⁻¹ for β -Cd(PO₃)₂ are designated as asymmetric O-P-O stretching vibrations. Symmetric O-P-O stretching vibrations are revealed by peaks at about 1118 cm⁻¹ and 1048 cm⁻¹ for the two compounds, respectively. Asymmetric stretching vibrations of P-O-P are demonstrated by absorption peaks at 942 cm⁻¹ for La(PO₃)₃, 944 cm⁻¹ for β -Cd(PO₃)₂, whereas those at 766 and 787 cm⁻¹ are attributed to symmetric P-O-P stretching vibrations. The fundamental frequency of the P-O group is characterized by peaks at around 526-568 cm⁻¹ for two compounds. IR spectra corroborate the existence of the [PO₃]_∞ chain, which is consistent with the consequence derived from the single-crystal XRD structural analyses and preceding announced phosphates.⁷¹

As presented in Figure 6c,f, the two compounds exhibit broad transmission. Particularly, the DUV cutoff edge of β -Cd(PO₃)₂ is <190 nm. The absorption data is converted from diffuse-reflectance data using the Kubelka–Munk function,

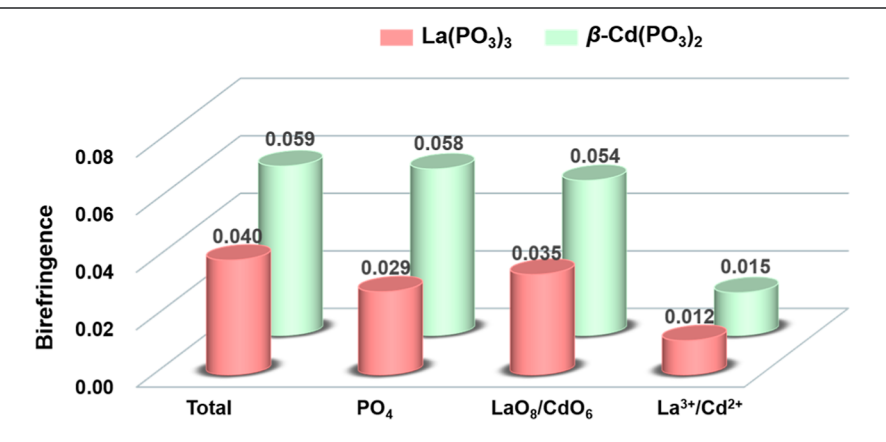


Figure 5. Birefringence of different groups in La(PO₃)₃ and β -Cd(PO₃)₂ obtained by the RSAC method.

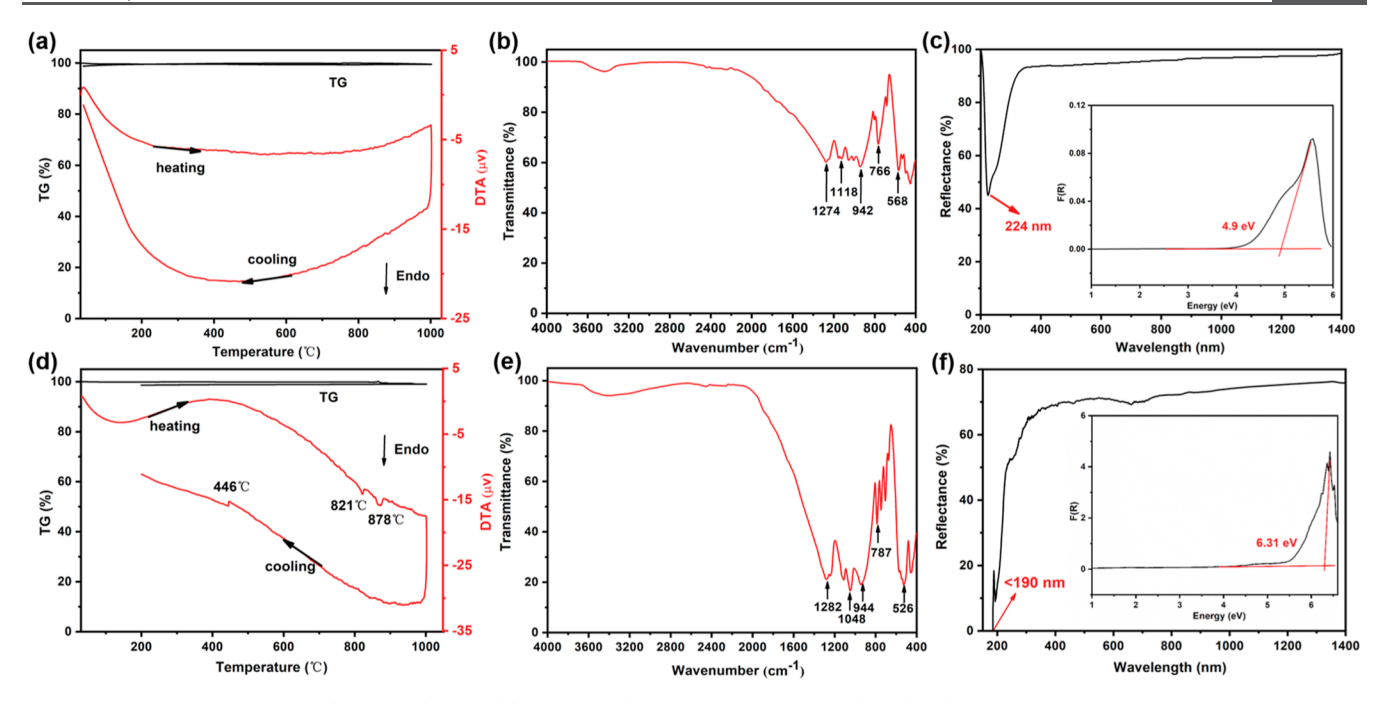


Figure 6. TG-DTA curves of (a) La(PO₃)₃ and (d) β -Cd(PO₃)₂. Infrared spectra of (b) La(PO₃)₃ and © β -Cd(PO₃)₂. UV-Vis-NIR diffuse reflectance spectra of (c) La(PO₃)₃ and (f) β -Cd(PO₃)₂.

 $F(R) = K/S = (1-R)^2/2R$, where K is absorption coefficient, S is scattering coefficient, and R is reflectance, 72,73 and its experimental band gap is 6.31 eV. Although Cd^{2+} with a d^{10} electronic structure can effectively inhibit the d-d electronic state, there are still very few Cd-based phosphates that can achieve DUV transmission. To our knowledge, β -Cd(PO_3)₂ has the shortest UV cutoff edge among all the reported Cd-based inorganic compounds and realizes equilibrium between a short cutoff edge and a large birefringence. Some representative Cd-based inorganics and their cutoff edges are shown in Table S10.

For the title compounds crystallized in NCS space groups, their SHG intensities are evaluated. As illustrated in Figure S3, β -Cd(PO₃)₂ is type-I phase-matchable based on the standard submitted by Kurtz and Perry. Its SHG intensity is \sim 0.25 × KDP, and SHG tensors were calculated as d_{14} = 0.195 pm/V and $d_{\rm eff}$ = 0.08 pm/V. However, the SHG measurement of La(PO₃)₃ shows feeble green light and about 1 × SiO₂ SHG intensity. The SHG tensor of La(PO₃)₃ is d_{14} = 0.005 pm/V, which conforms with the experimental result. In addition, the SHG-density map demonstrates P—O units providing fundamental contribution to the SHG effect of β -Cd(PO₃)₂, as shown in Figure S4.

3.5. Electronic Structure Calculations. With a view to further analyze the relationship between electronic structures and optical properties of $La(PO_3)_3$ and β -Cd($PO_3)_2$, the theoretical band structures are calculated. They are both direct band gap compounds at the G point, and their theoretical band gaps are 5.70 and 3.78 eV (Figure S5), which are smaller than the experimental values because of the underestimation of band gaps by the DFT method. As is known, the optical property of the material is principally determined by orbitals near the Fermi level. The calculated projected density of states (PDOS) showed (Figure S6) that the top of the valence band (VB) near the Fermi level and the bottom of the conduction band (CB) are primarily composed of O-2p, P-3p, and Cd-4d (La-5d) orbitals for β -Cd(PO_3)₂ and $La(PO_3)_3$, which is in

good agreement with the conclusion obtained by RSAC. It is indicated that in addition to main donor P-O groups, Cd-O, and La-O units also offer significant contribution to optical performances for the title compounds.

4. CONCLUSIONS

In summary, two NLO optical materials, namely, La(PO₃)₃ and β -Cd(PO₃)₂ have been synthesized through the hightemperature solution method. They both possess large birefringence and short cutoff edges, particularly for β -Cd(PO₃)₂; it has the largest birefringence (0.059 at 1064 nm) in DUV phosphates to date. The birefringence comes from the cooperation of P-O groups and the covalent impact of CdO₆ groups. Meanwhile, the P–O pseudolayer in β -Cd(PO₃)₂ is closer to planar arrangement, which also enhances optical anisotropy effectively. It is worth mentioning that β -Cd(PO₃)₂ possesses the shortest cutoff edge (<190 nm) among the reported Cd-based inorganic compounds and accomplishes balance between DUV transparence and large birefringence. These results demonstrate that metal phosphates are promising for exploring DUV NLO materials with a large birefringence in the future.

ASSOCIATED CONTENT

Supporting Information

The Supporting Information is available free of charge at https://pubs.acs.org/doi/10.1021/acs.chemmater.2c00825.

Atomic coordinates, equivalent isotropic displacement parameters, BVS calculations, bond lengths and angles, anisotropic displacement parameters, refractive indices, Mulliken population analysis, dipole moments, crystal photographs, energy-dispersive X-ray spectra, band structure and PDOS for La(PO₃)₃ and β -Cd(PO₃)₂, and SHG intensity and SHG density for β -Cd(PO₃)₂ (PDF)

Crystallographic information for La(PO₃)₃ (CIF)

Crystallographic information for β -Cd(PO₃)₂ (CIF)

Accession Codes

CCDC 2111018 (La(PO₃)₃) and 2111012 (β -Cd(PO₃)₂) contain the supplementary crystallographic data for this paper. These data can be obtained free of charge via www.ccdc.ca-m.ac.uk/data_request/cif.

AUTHOR INFORMATION

Corresponding Authors

Qun Jing — Xinjiang Key Laboratory of Solid State Physics and Devices, School of Physical Science and Technology, Xinjiang University, Urumqi 830046, China; ⊙ orcid.org/0000-0002-1801-2638; Email: qunjing@xju.edu.cn

Zhaohui Chen — Key Laboratory of Oil & Gas Fin Chemicals, Ministry of Education and Xinjiang Uyghur Autonomous Region, School of Chemical Engineering, Xinjiang University, Urumqi 830046, China; orcid.org/0000-0002-9472-2113; Email: chenzhaohui@xju.edu.cn

Authors

Jiarong Lv — Key Laboratory of Oil & Gas Fin Chemicals, Ministry of Education and Xinjiang Uyghur Autonomous Region, School of Chemical Engineering, Xinjiang University, Urumqi 830046, China

Yanyan Qian — Xinjiang Key Laboratory of Solid State Physics and Devices, School of Physical Science and Technology, Xinjiang University, Urumqi 830046, China

Xinmei Wang — Key Laboratory of Oil & Gas Fin Chemicals, Ministry of Education and Xinjiang Uyghur Autonomous Region, School of Chemical Engineering, Xinjiang University, Urumqi 830046, China

Ming-Hsien Lee — Department of Physics, Tamkang University, New Taipei City 25137, Taiwan; ⊚ orcid.org/ 0000-0003-3956-181X

Complete contact information is available at: https://pubs.acs.org/10.1021/acs.chemmater.2c00825

Author Contributions

J.L. and Y.Q. contributed equally. J.L. performed experiments, data analysis, and paper writing, and Y.Q. performed theoretical data analysis. X.W. performed performance test. M.-H.L. provided the method and software. Q.J., and Z.C. supervised all tasks. All authors contributed to the general discussion.

Notes

The authors declare no competing financial interest.

ACKNOWLEDGMENTS

This work was supported by the National Natural Science Foundation of China (grant nos. 51962033 and 11864040), the Graduate Research Innovation Project of Xinjiang Uyghur Autonomous Region (grant no. XJ2021G030), and the Tianshan Innovation Team Program of Xinjiang Uygur Autonomous Region (grant no. 2020D14038).

REFERENCES

- (1) Eaton, D. F. Nonlinear Optical Materials. Science 1991, 253, 281-287.
- (2) Becker, P. Borate Materials in Nonlinear Optics. Adv. Mater. 1998, 10, 979-992.
- (3) Mutailipu, M.; Poeppelmeier, K. R.; Pan, S. Borates: A rich source for optical materials. *Chem. Rev.* **2021**, *121*, 1130–1202.

- (4) Halasyamani, P. S.; Poeppelmeier, K. R. Noncentrosymmetric Oxides. *Chem. Mater.* **1998**, *10*, 2753–2769.
- (5) Rajamathi, M.; Seshadri, R. Oxide and chalcogenide nanoparticles from hydrothermal/solvothermal reactions. *Curr. Opin. Solid State Mater. Sci.* **2002**, *6*, 337–345.
- (6) Halasyamani, P. S.; Rondinelli, J. M. The must-have and nice-to-have experimental and computational requirements for functional frequency doubling deep-UV crystals. *Nat. Commun.* **2018**, *9*, 2972.
- (7) Ok, K. M. Toward the Rational Design of Novel Noncentrosymmetric Materials: Factors Influencing the Framework Structures. *Acc. Chem. Res.* **2016**, *49*, 2774–2785.
- (8) Tran, T. T.; Yu, H.; Rondinelli, J. M.; Poeppelmeier, K. R.; Halasyamani, P. S. Deep Ultraviolet Nonlinear Optical Materials. *Chem. Mater.* **2016**, 28, 5238–5258.
- (9) Xiong, L.; Chen, J.; Lu, J.; Pan, C.-Y.; Wu, L.-M. Monofluorophosphates: A New Source of Deep-Ultraviolet Nonlinear Optical Materials. *Chem. Mater.* **2018**, *30*, 7823–7830.
- (10) Zou, G.; Ok, K. M. Novel ultraviolet (UV) nonlinear optical (NLO) materials discovered by chemical substitution-oriented design. *Chem. Sci.* **2020**, *11*, 5404–5409.
- (11) Zhang, W.; Yu, H.; Wu, H.; Halasyamani, P. S. Phase-matching in nonlinear optical compounds: a materials perspective. *Chem. Mater.* **2017**, *29*, 2655–2668.
- (12) Chen, C.-t.; Liu, G.-z. Recent advances in nonlinear optical and electro-optical materials. *Annu. Rev. Mater. Sci.* **1986**, *16*, 203–243.
- (13) Chen, C.; Wu, Y.; Li, R. The anionic group theory of the nonlinear optical effect and its applications in the development of new high-quality NLO crystals in the borate series. *Int. Rev. Phys. Chem.* **1989**, *8*, 65–91.
- (14) Mutailipu, M.; Li, F.; Jing, C.; Yang, Z. H.; Poeppelmeier, K. R.; Pan, S. L. Strong nonlinearity induced by coaxial alignment of polar chain and dense [BO₃] units in CaZn₂(BO₃)₂. *Angew. Chem., Int. Ed.* **2022**, *61*, No. e202202096.
- (15) Zhao, S.; Gong, P.; Bai, L.; Xu, X.; Zhang, S.; Sun, Z.; Lin, Z.; Hong, M.; Chen, C.; Luo, J. Beryllium-free Li₄Sr(BO₃)₂ for deepultraviolet nonlinear optical applications. *Nat. Commun.* **2014**, *S*, 4019.
- (16) Xia, M.; Li, F.; Mutailipu, M.; Han, S.; Yang, Z.; Pan, S. Discovery of First Magnesium Fluorooxoborate with Stable Fluorine Terminated Framework for Deep-UV Nonlinear Optical Application. *Angew. Chem., Int. Ed.* **2021**, *60*, 14650–14656.
- (17) Zou, G.; Ye, N.; Huang, L.; Lin, X. Alkaline-alkaline earth fluoride carbonate crystals ABCO₃F (A = K, Rb, Cs; B = Ca, Sr, Ba) as nonlinear optical materials. *J. Am. Chem. Soc.* **2011**, *133*, 20001–20007
- (18) Yu, S.; Wu, H.; Yu, H.; Hu, Z.; Wang, J.; Wu, Y. $NH_4(B_6PO_{10}(OH)_4)H_2O$: exhibiting the largest birefringence in borophosphates. *Chem. Commun.* **2022**, *58*, 2834.
- (19) Shi, G.; Wang, Y.; Zhang, F.; Zhang, B.; Yang, Z.; Hou, X.; Pan, S.; Poeppelmeier, K. R. Finding the next deep-ultraviolet nonlinear optical material: NH₄B₄O₆F. *J. Am. Chem. Soc.* **2017**, *139*, 10645–10648.
- (20) Zhang, Z.; Wang, Y.; Zhang, B.; Yang, Z.; Pan, S. Polar fluorooxoborate, NaB_4O_6F : a promising material for ionic conduction and nonlinear optics. *Angew. Chem., Int. Ed.* **2018**, *57*, 6577–6581.
- (21) Wang, Y.; Zhang, B.; Yang, Z.; Pan, S. Cation-tuned synthesis of fluorooxoborates: towards optimal deep-ultraviolet nonlinear optical materials. *Angew. Chem., Int. Ed.* **2018**, *57*, 2150–2154.
- (22) Wang, X.; Wang, Y.; Zhang, B.; Zhang, F.; Yang, Z.; Pan, S. CsB_4O_6F : a congruent-melting deep-ultraviolet nonlinear optical material by combining superior functional units. *Angew. Chem., Int. Ed.* **2017**, *56*, 14119–14123.
- (23) Zhou, J.; Liu, Y.; Wu, H.; Yu, H.; Lin, Z.; Hu, Z.; Wang, J.; Wu, Y. $CsZn_2BO_3X_2$ (X = F, Cl and F & Cl): A series of beryllium-free deep ultraviolet nonlinear optical crystals with excellent properties. *Angew. Chem., Int. Ed.* **2020**, *59*, 19006–19010.
- (24) Peng, G.; Lin, C.; Ye, N. NaZnCO3(OH): A high-performance carbonate ultraviolet nonlinear optical crystal derived from KBe₂BO₃F₂. *J. Am. Chem. Soc.* **2020**, *142*, 20542–20546.

- (25) Liu, X.; Kang, L.; Gong, P.; Lin, Z. LiZn(OH)CO₃: A deepultraviolet nonlinear optical hydroxycarbonate designed from a diamond-like structure. *Angew. Chem., Int. Ed.* **2021**, *60*, 13574–13578.
- (26) Yu, P.; Wu, L.-M.; Zhou, L.-J.; Chen, L. Deep-Ultraviolet Nonlinear Optical Crystals: $Ba_3P_3O_{10}X$ (X = Cl, Br). *J. Am. Chem. Soc.* **2014**, 136, 480–487.
- (27) Zhao, S.; Gong, P.; Luo, S.; Bai, L.; Lin, Z.; Tang, Y.; Zhou, Y.; Hong, M.; Luo, J. Tailored synthesis of a nonlinear optical phosphate with a short absorption edge. *Angew. Chem., Int. Ed.* **2015**, *54*, 4217–4221
- (28) Chen, J.; Xiong, L.; Chen, L.; Wu, L.-M. Ba₂NaClP₂O₇: Unprecedented Phase Matchability Induced by Symmetry Breaking and Its Unique Fresnoite-Type Structure. *J. Am. Chem. Soc.* **2018**, *140*, 14082–14086.
- (29) Zhou, Y.; Zhang, X.; Xiong, Z.; Long, X.; Chen, Y.; Chen, X.; Zhao, S.; Lin, Z.; Luo, J.; Luo, J. H. Non- π -conjugated deepultraviolet nonlinear optical crystal $K_2Zn_3(SO_4)(HSO_4)_2F_4$. J. Phys. Chem. Lett. **2021**, 12, 8280–8284.
- (30) Wu, C.; Lin, L.; Wu, T.; Huang, Z.; Zhang, C. Deep-ultraviolet transparent alkali metal-rare earth metal sulfate $NaY(SO_4)_2 \cdot H_2O$ as a nonlinear optical crystal: synthesis and characterization. *CrystEng-Comm* **2021**, 23, 2945–2951.
- (31) Wen, X.; Lin, C.; Luo, M.; Fan, H.; Chen, K.; Ye, N. [C(NH₂)₃]₃PO₄·2H₂O: a new metal-free ultraviolet nonlinear optical phosphate with large birefringence and second-harmonic generation response. *Sci. China Mater.* **2021**, *64*, 2008–2016.
- (32) Zhao, S.; Gong, P.; Luo, S.; Bai, L.; Lin, Z.; Ji, C.; Chen, T.; Hong, M.; Luo, J. Deep-Ultraviolet Transparent Phosphates RbBa₂(PO₃)₅ and Rb₂Ba₃(P₂O₇)₂ Show Nonlinear Optical Activity from Condensation of [PO₄]³⁻ Units. *J. Am. Chem. Soc.* **2014**, *136*, 8560–8563.
- (33) Zhao, S.; Yang, X.; Yang, Y.; Kuang, X.; Lu, F.; Shan, P.; Sun, Z.; Lin, Z.; Hong, M.; Luo, J. Non-Centrosymmetric RbNaMgP₂O₇ with Unprecedented ThermoInduced Enhancement of Second Harmonic Generation. *J. Am. Chem. Soc.* **2018**, *140*, 1592–1595.
- (34) Zhang, X.; Wang, L.; Zhang, S.; Wang, G.; Zhao, S.; Zhu, Y.; Wu, Y.; Chen, C. Optical properties of the vacuum ultraviolet nonlinear optical crystal BPO₄. J. Opt. Soc. Am. B **2011**, 28, 2236–2239.
- (35) Cheng, H.; Li, F.; Yang, Z. H.; Pan, S. L. $Na_4B_8O_9F_{10}$:A novel deep-ultraviolet transparent nonlinear optical fluorooxoborate with unexpected short phase matching wavelength induced by optimized chromatic dispersion. *Angew. Chem., Int. Ed.* **2022**, 134, No. e202115669.
- (36) Baiheti, T.; Han, S.; Tudi, A.; Yang, Z.; Pan, S. Alignment of polar moieties leading to strong second harmonic response in KCsMoP₂O₉. *Chem. Mater.* **2020**, *32*, 3297–3303.
- (37) Baiheti, T.; Han, S.; Tudi, A.; Yang, Z.; Pan, S. Polar polymorphism: α -, and β -KCsWP₂O₉ nonlinear optical materials with strong second harmonic generation response. *J. Mater. Chem. C* **2020**, 8, 11441–11448.
- (38) Wu, B.-L.; Hu, C.-L.; Mao, F.-F.; Tang, R.-L.; Mao, J.-G. Highly polarizable Hg²⁺ induced a strong second harmonic generation signal and large birefringence in LiHgPO₄. *J. Am. Chem. Soc.* **2019**, *141*, 10188–10192.
- (39) Lu, X.; Chen, Z.; Shi, X.; Jing, Q.; Lee, M. H. Two Pyrophosphates with Large Birefringences and Second-Harmonic Responses as Ultraviolet Nonlinear Optical Materials. *Angew. Chem., Int. Ed.* **2020**, *59*, 17648–17656.
- (40) Qi, L.; Chen, Z.; Shi, X.; Zhang, X.; Jing, Q.; Li, N.; Jiang, Z.; Zhang, B.; Lee, M.-H. $A_3BBi(P_2O_7)_2$ (A = Rb, Cs; B = Pb, Ba): Isovalent cation substitution to sustain large second-harmonic generation responses. *Chem. Mater.* **2020**, 32, 8713–8723.
- (41) Yu, H.; Zhang, W.; Young, J.; Rondinelli, J. M.; Halasyamani, P. S. Bidenticity-enhanced second harmonic generation from Pb chelation in Pb₃Mg₃TeP₂O₁₄. *J. Am. Chem. Soc.* **2016**, *138*, 88–91.
- (42) Deng, Y.; Huang, L.; Dong, X.; Wang, L.; Ok, K. M.; Zeng, H.; Lin, Z.; Zou, G. K₂Sb(P₂O₇)F: Cairo pentagonal layer with

- bifunctional genes reveal optical performance. Angew. Chem., Int. Ed. 2020, 132, 21337–21342.
- (43) Seshadri, R.; Hill, N. A. Visualizing the Role of Bi 6s "Lone Pairs" in the Off-Center Distortion in Ferromagnetic BiMnO₃. *Chem. Mater.* **2001**, *13*, 2892–2899.
- (44) Zumsteg, F. C.; Bierlein, J. D.; Gier, T. E. KxRb1-xTiOPO₄: A new nonlinear optical material. *J. Appl. Phys.* **1976**, *47*, 4980–4985.
- (45) Driscoll, T. A.; Perkins, P. E.; Hoffman, H. J.; Stone, R. E. Efficient second-harmonic generation in KTP crystals. *J. Opt. Soc. Am. B* **1986**, *3*, 683–686.
- (46) SAINT. SAINT, version 7.60A; Bruker Analytical X-ray Instruments, Inc.: Madison, WI, 2008.
- (47) Sheldrick, G. M. Crystal structure refinement with SHELXL. Acta Crystallogr., Sect. C: Struct. Chem. 2015, 71, 3-8.
- (48) Spek, A. L. Single-crystal structure validation with the programPLATON. *J. Appl. Crystallogr.* **2003**, *36*, 7–13.
- (49) Loste, E.; Wilson, R. M.; Seshadri, R.; Meldrum, F. C. The role of magnesium in stabilising amorphous calcium carbonate and controlling calcite morphologies. *J. Cryst. Growth* **2003**, 254, 206–218
- (50) Kurtz, S. K.; Perry, T. T. A powder technique for the evaluation of nonlinear optical materials. *J. Appl. Phys.* **1968**, *39*, 3798–3813.
- (51) Clark, S. J.; Segall, M. D.; Pickard, C. J.; Hasnip, P. J.; Probert, M. I. J.; Refson, K.; Payne, M. C. First principles methods using CASTEP. Z. Kristallogr. Cryst. Mater. 2005, 220, 567–570.
- (52) Ceperley, D. M.; Alder, B. J. Ground state of the electron gas by a stochastic method. *Phys. Rev. Lett.* **1980**, 45, 566–569.
- (53) Perdew, J. P.; Burke, K.; Ernzerhof, M. Generalized Gradient Approximation Made Simple. *Phys. Rev. Lett.* **1996**, *77*, 3865–3868.
- (54) Kleinman, L.; Bylander, D. M. Efficacious form for model pseudopotentials. *Phys. Rev. Lett.* **1982**, *48*, 1425–1428.
- (55) Hamann, D. R.; Schlüter, M.; Chiang, C. Norm-conserving pseudopotentials. *Phys. Rev. Lett.* **1979**, 43, 1494–1497.
- (56) Nicholls, R. J.; Morris, A. J.; Pickard, C. J.; Yates, J. R. OptaDOS a new tool for EELS calculations. *J. Phys.: Conf. Ser.* **2012**, 371, 012062.
- (57) Morris, A. J.; Nicholls, R. J.; Pickard, C. J.; Yates, J. R. OptaDOS: A tool for obtaining density of states, core-level and optical spectra from electronic structure codes. *Comput. Phys. Commun.* **2014**, *185*, 1477–1485.
- (58) Lin, J.; Lee, M.-H.; Liu, Z.-P.; Chen, C.; Pickard, C. J. Mechanism for linear and nonlinear optical effects in β -BaB₂O₄ crystals. *Phys. Rev. B* **1999**, *60*, 13380–13389.
- (59) Matuszewski, J.; Kropiwnicka, J.; Znamierowska, T. The crystal structure of lanthanum metaphosphate LaP₃O₉. *J. Solid State Chem.* **1988**, 75, 285–290.
- (60) Bagieu-Beucher, M.; Brunel-Laügt, M.; Guitel, J. C. Structure cristalline de la forme de haute temperature du polyphosphate de cadmium Cd(PO₃)₂-beta. *Acta Crystallogr., Sect. B: Struct. Sci.* **1979**, 35, 292–295.
- (61) Sun, T.; Shan, P.; Chen, H.; Liu, X.; Liu, H.; Chen, S.; Cao, Y. a.; Kong, Y.; Xu, J. Growth and properties of a noncentrosymmetric polyphosphate CsLa(PO₃)₄ crystal with deepultraviolet transparency. *CrystEngComm* **2014**, *16*, 10497–10504.
- (62) Shan, P.; Sun, T.; Chen, H.; Liu, H.; Chen, S.; Liu, X.; Kong, Y.; Xu, J. Crystal growth and optical characteristics of beryllium-free polyphosphate, KLa(PO₃)₄, a possible deep-ultraviolet nonlinear optical crystal. *Sci. Rep.* **2016**, *6*, 25201.
- (63) Yu, H.; Young, J.; Wu, H.; Zhang, W.; Rondinelli, J. M.; Halasyamani, P. S. $M_4Mg_4(P_2O_7)_3$ (M=K, Rb): Structural Engineering of Pyrophosphates for Nonlinear Optical Applications. *Chem. Mater.* **2017**, 29, 1845–1855.
- (64) Bai, Z.; Liu, L.; Zhang, L.; Huang, Y.; Yuan, F.; Lin, Z. $K_2SrP_4O_{12}$: a deep-UV transparentcyclophosphate as a nonlinear optical crystal. *Chem. Commun.* **2019**, *55*, 8454–8457.
- (65) Kliner, D. A. V.; Di Teodoro, F.; Koplow, J. P.; Moore, S. W.; Smith, A. V. Efficient second, third, fourth, and fifth harmonic generation of a Yb-doped fiber amplifier. *Opt. Commun.* **2002**, *210*, 393–398.

- (66) Lu, J.; Yue, J.-N.; Xiong, L.; Zhang, W.-K.; Chen, L.; Wu, L.-M. Uniform Alignment of Non-π-Conjugated Species Enhances Deep Ultraviolet Optical Nonlinearity. *J. Am. Chem. Soc.* **2019**, *141*, 8093–8097.
- (67) Lin, J.; Lee, M.-H.; Liu, Z.-P.; Chen, C.; Pickard, C. J. Mechanism for linear and nonlinear optical effects in β -BaB₂O₄ crystals. *Phys. Rev. B* **1999**, *60*, 13380.
- (68) Shu, S.; Huang, J.; Hu, C.; Pan, S. L.; Yang, Z. H. Hierarchical modulation on optical anisotropy driven by metal cation polyhedra in fluorooxoborates $M^{II}B_4O_6F_2$ (M^{II} = Be, Mg, Pb, Zn, Cd). *Chem.—Eur. J.* **2022**, 28, No. e202103401.
- (69) Pauling, L. The Nature of the Chemical Bond; Cornel University Press: Ithaca, NY, 1960; p 126.
- (70) Debye, P. *Polar Molecules*; The Chemical Catalog Co., Inc.: New York, 1929; p 172.
- (71) Yu, T.; Xiong, L.; Liu, X.; Yang, Y.-C.; Lin, Z.; Wu, L.-M.; Chen, L. $AZn(PO_3)_3$ (A = K, Rb): deep-ultraviolet nonlinear optical phosphates derived from synergy of a unique [ZnO₆] octahedron and a [PO₃]_∞ chain. *Cryst. Growth Des.* **2021**, *21*, 2445–2452.
- (72) Kubelka, P.; Munk, F. Z. An Article on Optics of Paint Layers. Z. Tech. Phys. 1931, 12, 259.
- (73) Tauc, J. Absorption edge and internal electric fields in amorphous semiconductors. *Mater. Res. Bull.* **1970**, *5*, 721–729.

☐ Recommended by ACS

One-Side Capping in Two-Dimensional WO₃-Type Materials Leading to Strong Second-Harmonic Response

Haonan Liu, Hongwei Yu, et al.

MARCH 29, 2022

CHEMISTRY OF MATERIALS

READ 🗹

Tunable Circularly Polarized Luminescence from Single Crystal and Powder of the Simplest Tetraphenylethylene Helicate

Ming Hu, Yan-Song Zheng, et al.

SEPTEMBER 21, 2021

ACS NANO

READ **C**

Mechanism of Different Piezoresponsive Luminescence of 2,3,4,5-Tetraphenylthiophene and 2,3,4,5-Tetraphenylfuran: A Strategy for Designing Pressure...

Yarong Gu, Bo Zou, et al.

JANUARY 08, 2020

THE JOURNAL OF PHYSICAL CHEMISTRY LETTERS

READ 🗹

Pressure Controls the Structure and Nonlinear Optical Properties of Piezochromic CdTeMoO $_6$

Dequan Jiang, Yonggang Wang, et al.

APRIL 07, 2021

CHEMISTRY OF MATERIALS

READ 🗹

Get More Suggestions >